Bestowing Antifungal and Antibacterial Activities by Lipophilic Acid Conjugation to D,L-Amino Acid-Containing Antimicrobial Peptides: A Plausible Mode of Action†

Dorit Avrahami and Yechiel Shai*

Department of Biological Chemistry, The Weizmann Institute of Science, Rehovot, 76100 Israel

Received July 2, 2003; Revised Manuscript Received October 12, 2003

ABSTRACT: The dramatically increased frequency of opportunistic fungal infections has prompted research to diversify the arsenal of antifungal agents. Antimicrobial peptides constitute a promising family for future antibiotics with a new mode of action. However, only a few are effective against fungal pathogens because of their ability to self-assemble. Recently, we showed that the conjugation of fatty acids to the potent antibacterial peptide magainin endowed it with antifungal activity concomitant with an increase in its oligomeric state in solution. To investigate whether a high potency of the parental peptide is prerequisite for antifungal activity, we conjugated undecanoic acid (UA) and palmitic acid (PA) to inactive diastereomers of magainin containing four D-amino acids ([D]-4-magainin), as well as to a weakly active diastereomeric lytic peptide containing Lys and Leu ([D]-K_5L_7). All lipopeptides gained potent activity toward *Cryptococcus neoformans*. Most importantly, [D]-K_5L_7-UA was highly potent against all microorganisms tested, including bacteria, yeast, and opportunistic fungi. All lipopeptides increased the permeability of *Escherichia coli* spheroplasts and intact *C. neoformans*, as well as their corresponding membranes, phosphatidylethanol (PE)/phosphatidylglycerol (PG) and phosphatidylcholine (PC)/PE/phosphatidylinositol (PI)/ergosterol, respectively. The extent of membrane-permeating activity correlated with their biological function, suggesting that the plasma membrane was one of their major targets. Circular dichroism (CD) and attenuated total reflectance Fourier transform infrared (ATR-FTIR) spectroscopy revealed that their mode of oligomerization in solution, structure, and organization in membranes have important roles regarding their antibacterial and antifungal activities. Together with the advantage of using diastereomers versus all L-amino acid peptides, this study paves the way to the design of a new group of potent antifungal peptides urgently needed to combat opportunistic fungal infection.

In the past decade, the frequency of opportunistic fungal infections has increased dramatically. Generally, the spectrum of fungal pathogens has changed, although the vast majority of the invasive fungal infections are still due to *Aspergillus* and *Candida* species (*1*−*3*). Azoles that inhibit sterol formation and polyenes that bind to mature membrane sterols have been the mainstays of antifungal therapy for two decades or more (*4*, *5*). However, the emergence of fluconazole resistance among different pathogenic strains and the high toxicity of amphotericin B (*6*, *7*) have prompted research on new antifungal agents (*8*). One group of agents that has received some attention is that of native lipopeptides, which possess a broad spectrum of activities, including antibacterial, antifungal, antiviral, and cytolytic activities (*9*−*13*; reviewed in ref *14*). These lipopeptides are produced nonribosomally, in bacteria, yeast, or fungi, during cultivation on various carbon sources (*15*−*17*). Structurally, most of them have a unique alkyl chain bound to a short peptide chain (6−7 amino acids), a cyclic structure (*18*), and composed mainly of hydrophobic and acidic L- and D-amino acids. Their mode of action is either via nonspecific membrane lysis, e.g., iturin (*19*) and surfactin (*20*), or via inhibition of the synthesis of cell wall components, e.g., the echinocandins family, which inhibit the synthesis of 1,3-β-D-glucan (*21*) (reviewed in ref *8*). One of the most important members in the echinocandins family is caspofungin, which has been approved recently by the FDA for clinical usage (*22*, *23*).

Promising alternatives to these lipopeptides are cationic antimicrobial peptides that serve as part of the innate immunity of all organisms (*24*−*27*). Some kill specifically bacteria, fungi or both, whereas others are also highly toxic to mammalian cells (*28*−*34*). Despite extensive studies, the molecular mechanism for their target specificity is still not clear. However, it has been shown that antifungal peptides bind and permeate efficiently both zwitterionic and negatively charged phospholipid membranes and that they self-associate in solution and/or in membranes (reviewed in ref *34*). Self-association is driven either by a hydrophobic N- or C-terminus or by specific amino acids in the peptide sequence, resulting in the formation of α-helical bundles that could possibly initiate strong hydrophobic binding to zwitterionic membranes (*29*, *31*, *35*, *36*). Alternatively, monomers were covalently linked via a template (*37*). In view of this, a new approach was utilized to increase the peptides' hydrophobicity and ability to self-associate, without altering

† This study was supported by the Israel Science Foundation. Y.S. holds the Harold S. and Harriet B. Brady Professorial Chair in Cancer Research.

* To whom correspondence should be addressed: Tel 972-8-9342711; fax 972-8-9344112; e-mail Yechiel.Shai@weizmann.ac.il.

10.1021/bi035142v CCC: $25.00
Published on Web 11/22/2003

the properties of the peptidic chain. This has been done by attaching lipophilic acids of different lengths to the N-terminus of magainin, a potent antimicrobial peptide selective for bacteria (*38*). A direct correlation was found between oligomerization of the lipopeptides in solution and potent antifungal activity; only oligomeric lipopeptides were antifungal. To investigate whether a high potency of the parental peptide is a prerequisite for antifungal activity, we analyzed the effects of lipophilic acid conjugation to inactive or weakly active diastereomeric (containing both L- and D-amino acids) peptides. The advantages of diasteremoric antimicrobial peptides compared with their parental all-L-amino acid peptides have been reported and reviewed (*39*, *40*). Unfortunately, the incorporation of D-amino acids into native antimicrobial peptides or mildly hydrophobic amphipathic α-helical peptides abolished or significantly reduced their activities, most probably due to drastic destabilization of their amphipathic structure. Here we selected two diastereomers, one of a de novo-designed K,L-containing 12-mer peptide and the second one of magainin, a 23 amino acid native antimicrobial peptide. The positions of the D-amino acids along the peptides' sequence were selected to maximally disrupt the helical structure. The N-terminus of each peptide was conjugated with either undecanoic acid (UA)[1] or palmitic acid (PA), both of which can induce peptide oligomerization in solution. The diastereomeric lipopeptides were evaluated with regard to their cytotoxicity against yeast, fungi, bacteria, and human erythrocytes, as well as their ability to depolarize the transmembrane potential of living microorganisms and model vesicles. Their plausible mode of action was studied by using ATR-FTIR[1] and CD[1] spectroscopy, transmission electron microscopy, and ability to increase the permeability of model membranes and live bacteria and fungi. The ability of lipophilic acid conjugation to restore partial or potent antibacterial and antifungal activity of inactive/weakly active diastereomeric peptides, irrespective of their size and the specific sequence, is discussed with regard to their structure, oligomeric state, and ability to permeate the target cell membrane.

MATERIALS AND METHODS

Materials. Rink amide MBHA resin, 4-methylbenzhydrylamine resin (BHA), and 9-fluorenylmethoxycarbonyl (Fmoc) amino acids were obtained from Calbiochem−Novabiochem AG (Switzerland). Other reagents used for peptide synthesis included trifluoroacetic acid (TFA, Sigma), piperidine (Merck), *N*,*N*-diisopropylethylamine (DIEA, Sigma), *N*-methylmorpholine (NMM, Fluka), *N*-hydroxybenzotriazole hydrate (HOBT, Aldrich), 2-(1*H*-benzotriazol-1-yl)-1,1,3,3-tetramethyluronium hexafluorophosphate (HBTU), and dimethylformamide (DMF, peptide synthesis grade, Biolab). Phosphatidylcholine (PC, from egg yolk), phosphatidylethanolamine (PE, from *Escherichia coli*), phosphatidylinositol (PI, from bovine liver), and ergosterol were purchased from Sigma. 3,3′-Dipropylthiadicarbocyanine iodide (DiS-C_3-5), and Calcein were purchased from Molecular Probes (Junction City, OR). All other reagents were of analytical grade. Buffers were prepared in double-distilled water. Amphotericin B was purchased from Sigma Chemical Co. (Israel). RPMI 1640 was purchased from Biological Industries (Beit Haemek, Israel).

Peptide Synthesis, Acylation, and Purification. Peptides were synthesized by a fluoren-9-ylmethoxylcarbonyl (Fmoc) solid-phase method on Rink amide MBHA resin, by use of a ABI 433A automatic peptide synthesizer. The lipophilic acid was attacched to the N-terminus of a resin-bound peptide by standard Fmoc chemistry. Briefly, after removal of the Fmoc from the N-terminus of the peptide with a solution of 20% piperidine in DMF, the fatty acid [7 equiv (1 M in DMF)] was coupled to the resin under similar conditions used for the coupling of an amino acid. The peptides were cleaved from the resin by 95% trifluoroacetic acid (TFA) and were purified by RP-HPLC (reverse-phase high-performance liquid chromatography) on a C_{18} (for nonlipidic peptides) or C_4 (for the lipopeptides) Bio-Rad semipreparative column (250 × 10 mm, 300 Å pore size, 5 μm particle size). The purified peptides were shown to be homogeneous (>98%) by analytical RP-HPLC. The elution time of the lipopeptides increased by ∼20 min, indicating an increase in hydrophobicity due to the attachment of the fatty acid. Electrospray mass spectroscopy was used to confirm their molecular weight, and amino acid analysis was used to confirm the composition of the peptidic moiety.

Antifungal and Antibacterial Activities of the Peptides. The antifungal activity of the peptides and their lipophilic acid-conjugated analogues was measured according to the conditions of NCCLS document M27-A. The peptides were examined in sterile 96-well plates (Nunc F96 microtiter plates) in a final volume of 200 μL as follows: 100 μL of a suspension containing fungi at a concentration of 2×10^3 colony-forming units (CFU)/mL in culture medium (RPMI 1640, 0.165 M MOPS, pH 7.0, with L-glutamine, without $NaHCO_3$ medium) was added to 100 μL of water containing the peptide in serial 2-fold dilutions. The fungi were incubated for 24 h in the case of *Aspergillus fumigatus* or 48−72 h for *Candida albicans* and *Cryptococcus neoformans* at 35°C in a Binder KB115 incubator. Growth inhibition was determined by measuring the absorbance at 620 nm in a microplate autoreader El309 (Bio-tek Instruments). Antifungal activity was expressed as the minimal inhibitory concentration (MIC), the minimal concentration at which no growth was observed. The fungi used were *A. fumigatus* ATCC 26430, *C. albicans* ATCC 10231, and *C. neoformans* ATCC MYA-422.

The antibacterial activity of the peptides and their lipophilic acid-conjugated analogues was examined in sterile 96-well plates (Nunc F96 microtiter plates) in a final volume of 100 μL as follows. Aliquots (50 μL) of a suspension containing bacteria, at a concentration of 10^6 colony-forming units (CFU)/mL in culture medium (LB medium), were added to 50 μL of water containing the peptide in serial 2-fold dilutions in LB. Inhibition of growth was determined by measuring the absorbance at 492 nm with a microplate autoreader El309 (Bio-tek Instruments), after an incubation of 18−20 h at 37 °C. Antibacterial activities were expressed as the minimal inhibitory concentration (MIC), the minimal concentration at which no growth was observed after 18−

[1] Abbreviations: ATR-FTIR, attenuated total reflectance Fourier transform infrared; CD, circular dichroism; CFU, colony-forming units; hRBC, human red blood cells; PBS, phosphate-buffered saline; PI, phosphatidylinositol; PE, phosphatidylethanolamine; PC, phosphatidylcholine; PG, phosphatidylglycerol; RP-HPLC, reverse-phase high-performance liquid chromatography; UA, undecanoic acid; PA, palmitic acid.

20 h of incubation. The bacteria used were *E. coli* ATCC 25922, *Pseudomonas aeruginosa* ATCC 27853, *Bacillus subtilis* ATCC 6051, and *Staphylococcus aureus* ATCC 6538P.

Hemolytic Activity of the Peptides. Fresh hRBC with EDTA were rinsed 3 times with PBS (35 mM phosphate buffer/0.15 M NaCl, pH 7.3) by centrifugation for 10 min at 800*g* and resuspended in PBS. Peptides dissolved in PBS were then added to 50 μL of a solution of the stock hRBC in PBS to reach a final volume of 100 μL (final erythrocyte concentration 4% v/v). The resulting suspension was incubated under agitation for 60 min at 37 °C. The samples were then centrifuged at 800*g* for 10 min. The release of hemoglobin was monitored by measuring the absorbance of the supernatant at 540 nm. Controls for zero hemolysis (blank) and 100% hemolysis consisted of hRBC suspended in PBS and Triton 1%, respectively.

Preparation of Liposomes. Small unilamellar vesicles (SUV) were prepared by sonication as described earlier (*41*). Briefly, dry lipids were dissolved in $CHCl_3$/MeOH (2:1 v/v). The solvents were then evaporated under a stream of nitrogen and the lipids were lyophilized overnight. The lipids were resuspended in the appropriate buffer (7 mg/mL) with vortexing, and the resulting lipid dispersions were sonicated (10−30 min) in a bath-type sonicator (G1125SP1 sonicator, Laboratory Supplies Company, Inc.) until the turbidity had cleared. Vesicles were visualized on a JEOL JEM 100B electron microscope (Japan Electron Optics Laboratory Co., Tokyo, Japan). Lipid films were prepared from two types of phospholipids, PC/PE/PI/ergosterol (5:2.5:2.5:1 w/w/w/w) and PE/PG (7:3 w/w), which mimic the outer leaflet of the plasma membranes of *C. albicans* (*42*) and *E. coli*, respectively.

Circular Dichroic Spectroscopy. The CD spectra of the peptides were measured in an Aviv 202 spectropolarimeter. The spectra were scanned with a thermostated quartz optical cell with a path length of 1 mm. Each spectrum was recorded with an average time of 5 s, and 0.2 nm/s, at a wavelength range of 260−190 nm. The peptides were scanned at a concentration of 10−100 μM in PBS (35 mM phosphate buffer, without Ca^{2+} and Mg^{2+}, and 0.15 M NaCl, pH 7.3). Fractional helicities (*43*, *44*) were calculated as follows:

$$\frac{[\theta]_{222} - [\theta]_{222}{}^{0}}{[\theta]_{222}{}^{100} - [\theta]_{222}{}^{0}}$$

where $[\theta]_{222}$ is the experimentally observed mean residue ellipticity at 222 nm and values for $[\theta]_{222}{}^{0}$ and $[\theta]_{222}{}^{100}$, corresponding to 0% and 100% helix content at 222 nm, are estimated to be −2000 and −32 000 deg·cm^2/dmol, respectively (*43*).

Increase in Membrane Permeability Induced by the Peptides Measured by a Diffusion Potential Assay. Membrane destabilization, which results in the collapse of a diffusion potential, was detected fluorometrically for both living cells and model vesicles. Membrane destabilization, which results in the collapse of transmembrane potential, was detected fluorometrically by use of a fluorescence dye (*45*). The dye binds the plasma membrane due to the cell transmembrane potential or the induced transmembrane potential in the vesicles, resulting in a quenching of the dye's fluorescence. Peptide-induced membrane permeation caused a dissipation of the transmembrane potential that was monitored by an increase in fluorescence due to the release of the dye. Experiments were performed in sterile 96-well plates (Nunc F96 microtiter plates) in a final volume of 100 μL, as follows: 50 μL of vesicles/cells and the dye (diS-C_3-5) were added to 50 μL of the proper buffer containing the peptide in serial 2-fold dilutions. Peptide-induced membrane permeation caused a dissipation of the diffusion potential. Diffusion potential was monitored by an increase in the dye's fluorescence on a Molecular Devices, Spectra Max Gemini fluorometer. Fluorescence was monitored with excitation and emission wavelengths at 622 and 670 nm, respectively. The percentage of fluorescence recovery, F_t, was defined by

$$F_t = [(I_t - I_0)/(I_f - I_0)] \times 100$$

where I_t = fluorescence observed after the addition of a peptide at time t; I_0 = fluorescence after the binding of the dye to the membrane, reaching the minimum baseline; and I_f = the maximum fluorescence induced by a positive control peptide such as native melitin.

(*i*) *Potential Depolarization Assay with Model Vesicles.* The assay was performed as previously described (*39*, *41*, *45*, *46*). Briefly, a liposome suspension, prepared in K^+ buffer (50 mM K_2SO_4/25 mM HEPES sulfate, pH 6.8), was added to an isotonic K^+-free buffer (50 mM Na_2SO_4/25 mM HEPES sulfate, pH 6.8), containing 1 μM diS-C_3-5 dye. The subsequent addition of 1 pM valinomycin created a negative diffusion potential inside the vesicles by a selective efflux of K^+ ions, which resulted in a quenching of the dye's fluorescence. The experiments were performed in isotonic K^+-free buffer containing the peptides in serial 2-fold dilutions.

(*ii*) *Potential Depolarization Assay with Intact Yeast.* Intact yeast cells of the sensitive *C. neoformans* were used similarly to what has been described previously (*38*). Cells were centrifuged at 2500 rpm for 5 min at 4 °C after being incubated at 35 °C with agitation for 4 h (log phase) in RPMI buffer (RPMI 1640, 0.165 M MOPS, pH 7.0, with L-glutamine and without $NaHCO_3$). The cells were resuspended in PBS (without Ca^{2+} and Mg^{2+}) to an inoculum of 2×10^5 CFU/mL. The cells were incubated with 1 μM diS-C_3-5 followed by fluorescence dequenching until a stable baseline was achieved (∼5 min), indicating the binding of the dye onto the yeast membrane surface. Experiments were performed in PBS containing the peptides in serial 2-fold dilutions.

(*iii*) *Potential Depolarization Assay with Bacterial Spheroplasts.* The assay was performed as described previously (*37*). Spheroplasts of the Gram-negative bacteria *E. coli* D21 were prepared by osmotic shock procedure (*47*). Bacteria were grown at 37 °C with agitation to mid-log phase. Cells from grown cultures (OD_{600} = 0.8) were harvested by centrifugation and washed twice with 10 mM Tris/H_2SO_4 and 25% sucrose, pH 7.5. Cells were resuspended in the washing buffer containing 1 mM EDTA. After 10 min of incubation at 20 °C with rotary mixing, the cells were collected by centrifugation and resuspended immediately in ice-cold water. After 10 min of incubation at 4 °C with rotary mixing, the spheroplasts were collected by centrifugation. The

spheroplasts were then resuspended to OD_{600} 0.05 in a buffer containing spheroplasts buffer (20 mM glucose, 5 mM HEPES, and 1 M KCl, pH 7.3). The cells were incubated with 1 μM diS-C_3-5, followed by fluorescence dequenching until a stable baseline was achieved ($\sim$ 2 h), indicating the binding of the dye onto the bacteria membrane surface. Experiments were performed in bacteria spheroplast buffer containing the peptide in serial 2-fold dilutions.

ATR-FTIR Spectroscopy. Spectra were obtained on a Bruker equinox 55 FTIR spectrometer equipped with a deuterated triglyceride sulfate (DTGS) detector and coupled with an ATR device. For each spectrum, 150 scans were collected, with a resolution of 4 cm^{-1}. Samples were prepared as previously described (*48*). Briefly, lipids alone or with a peptide were deposited on a ZnSe horizontal ATR prism (80 $\times$ 7 mm). Prior to sample preparations, the trifluoroacetate (CF_3COO^-) counterions, which strongly associate with the peptide, were replaced with chloride ions by several washings in 0.1 M HCl followed by lyophilization. This allowed the elimination of the strong C=O stretching absorption band near 1673 cm^{-1} (*49*). Peptides were dissolved in MeOH and lipids in a 1:2 MeOH/$CHCl_3$ mixture. Lipid−peptide mixtures or lipids with the corresponding volume of methanol were spread with a Teflon bar on the ZnSe prism. The solvents were eliminated by drying under vacuum for 30 min. Pure phospholipid spectra were subtracted to yield the difference spectra. The background for each spectrum was a clean ZnSe prism. Hydration of the sample was achieved by introducing an excess of deuterium oxide (D_2O) into a chamber placed on top the ZnSe prism in the ATR casting and incubating for 4 min prior to the acquisition of spectra. H/D exchange was considered complete due to the complete shift of the amide II band. Any contribution of D_2O vapor to the absorbance spectra near the amide I peak region was eliminated by subtraction of the spectra of pure lipids equilibrated with D_2O under the same conditions.

ATR-FTIR Data Analysis. To resolve overlapping bands, the spectra were processed with PEAKFIT (Jandel Scientific, San Rafael, CA) software. Second-derivative spectra were calculated to identify the positions of the component bands in the spectra. These wavenumbers were used as initial parameters for curve fitting with Gaussian component peaks. Positions, bandwidths, and amplitudes of the peaks were varied until good agreement between the calculated sum of all components and the experimental spectra was achieved ($r^2 > 0.999$). The relative amounts of different secondary structure elements were estimated by dividing the areas of individual peaks, assigned to a particular secondary structure, by the whole area of the resulting amide I band.

Analysis of the Polarized ATR-FTIR Spectra. The ATR electric fields of incident light were calculated as follows (*50*, *51*):

$$E_x = \frac{2\cos\theta\sqrt{\sin^2\theta - {n_{21}}^2}}{\sqrt{(1-{n_{21}}^2)[(1+{n_{21}}^2)\sin^2\theta - {n_{21}}^2]}}$$

$$E_y = \frac{2\cos\theta}{\sqrt{1-{n_{21}}^2}}$$

$$E_z = \frac{2\sin\theta\cos\theta}{\sqrt{(1-{n_{21}}^2)[(1+{n_{21}}^2)\sin^2\theta - {n_{21}}^2]}}$$

where θ is the angle of a light beam to the prism, normal at the point of reflection (45°), and $n_{21} = n_2/n_1$ (n_1 and n_2 are the refractive indices of ZnSe, taken as 2.4, and the membrane sample, taken as 1.5, respectively). Under these conditions, E_x, E_y, and E_z are 1.09, 1.81, and 2.32, respectively. The electric field components, together with the dichroic ratio [defined as the ratio between the absorption of parallel (to a membrane plane), A_p, and perpendicularly polarized incident light, A_s] are used to calculate the orientation order parameter, *f*, by the following formula:

$$f = \frac{2({E_x}^2 - R^{ATR}{E_y}^2 + {E_z}^2)}{h(3\cos^2\alpha - 1)({E_x}^2 - R^{ATR}{E_y}^2 - 2{E_z}^2)}$$

where α is the angle between the transition moment of the amide I vibration of an α-helix and the helix axis. Several values ranging from 27° to 40° were reported in the literature for α (*52*). We used the values of 27° (*50*, *53*) and 39° (*54*) for α. Lipid order parameters were obtained from the symmetric ($\sim$2853 cm^{-1}) and antisymmetric ($\sim$2922 cm^{-1}) lipid stretching modes by use of the same equations, setting $\alpha = 90°$ (*50*).

Examination of Bacterial Membrane Damage by Transmission Electron Microscopy. Samples containing *E. coli* ATCC 25922 (1×10^6 CFU/mL) in LB medium were incubated with the lipopeptides at their MIC for 15 min. A drop containing the bacteria was deposited onto a carbon-coated grid and negatively stained with 2% phosphotungstic acid (PTA), pH 6.8. The grids were examined on a JEOL JEM 100B electron microscope (Japan Electron Optics Laboratory Co., Tokyo, Japan).

RESULTS

Peptides Design. Diastereomers of magainin-2 (23 amino acid) and a short model peptide (12 amino acid) composed of lysine and leucine were synthesized and conjugated to either undecanoic acid (UA) [CH_3-$(CH_2)_9$-COOH] or palmitic acid (PA) [CH_3-$(CH_2)_{14}$-COOH]. The short diastereomeric peptide ([D]-K_5L_7) was designed to create a perfect amphipathic α-helical structure in its L-form, based on Schiffer and Edmondson's wheel projection (*55*), similar to native magainin-2. The lipopeptides were investigated for their biological activity and a plausible mode of action. The sequences of the peptides, their designations, and net charge are shown in Table 1.

Antifungal, Antibacterial, and Hemolytic Activity of the Peptides. Antifungal activity was assayed against representative pathogenic fungi and yeast that commonly infect immunocompromised individuals. The antifungal drug amphotericin B served as a control, and its activity was similar to previously reported MIC values. MIC values of the peptides toward *C. albicans*, *C. neoformans*, and *A. fumigatus* are shown in Table 2. The data reveal that all the lipopeptides, including the parental peptide [D]-K_5L_7, were highly active toward *C. neoformans*. Most interestingly, [D]-K_5L_7-UA became highly potent toward all fungi and yeast tested,

Table 1: Peptide Sequences and Designations[a]

peptide formula	peptide designation	sequence	net charge	molecular weight
[D]-$L^{3,4,8,10}$-K_5L_7	[D]-K_5L_7	KK**LL**KLL**L**KL**L**LK-NH_2	+5	1450
[D]-L^{6}-K^{10}-F^{16}-E^{19}magainin	[D]-4-magainin	GI**G**K**F**L**L**HSA**K**KWGKA**F**VG**E**IMNS-NH_2	+4	2504

[a] Boldface underlined letters indicate D-amino acids. The C-terminus of all the peptides is amidate.

Table 2: Minimal Inhibitory Concentration of the Peptides toward Yeast and Fungi[a]

	minimal inhibitory concn (μM)			
	yeast		fungi	
peptide designation	*C. albicans* (ATCC 10231)	*C. neoformans* (ATCC MYA-422)	*A. fumigatus* (ATCC 26430)	% hemolytic activity at maximal MIC
[D]-K_5L_7	>50	12.5	>50	0
[D]-K_5L_7-UA	3.1	1.5	6.2	10
[D]-K_5L_7-PA	>50	3.1	3.1	2
[D]-4-magainin	>50	>50	>50	
[D]-4-magainin-UA	>50	6.2	>50	2
[D]-4-magainin-PA	>50	6.2	>50	8

The results are the mean of three independent experiments, each performed in duplicate, with a standard deviation of 25%. For the peptides' sequences, see Table 1.

Table 3: Minimal Inhibitory Concentration of the Peptides toward Gram-Negative and Gram-Positive Bacteria[a]

	minimal inhibitory concn (μM)			
	Gram negative		Gram positive	
peptide designation	*E. coli* ATCC 25922	*P. aeruginosa* ATCC 27853	*B. subtilis* ATCC 6051	*S. aureus* ATCC 6538P
[D]-K_5L_7	>50	25	3.1	>50
[D]-K_5L_7-UA	6.2	3.1	1.5	3.1
[D]-K_5L_7-PA	>50	>50	25	>50
[D]-4-magainin	>50	>50	50	>50
[D]-4-magainin-UA	>50	50	6.2	50
[D]-4-magainin-PA	>50	>50	50	>50

The results are the mean of three independent experiments, each performed in duplicate, with a standard deviation of 25%. For the peptides' sequences, see Table 1.

although the parental peptide was active only on the strain of *C. neoformans* tested.

The parental peptides and their lipopeptide conjugates were tested also against two Gram-negative bacteria (*E. coli* and *P. aeruginosa*) and two Gram-positive bacteria (*B. subtilis* and *S. aureus*) (Table 3). Interestingly, [D]-K_5L_7-UA was potent also toward all bacteria tested, with MICs similar to those obtained with fungi, despite the fact that the bacterial membrane is highly negatively charged compared with the zwitterionic composition of the membrane of fungi and yeast. However, the palmitoylated [D]-K_5L_7-PA was practically inactive on bacteria, in contrast to its high activity toward *C. neoformans* and *A. fumigatus*. This indicates that factors other than lipophilic tail length and peptide hydrophobicity are involved in peptide antimicrobial activity and will be discussed in the following paragraphs.

We tested the lipopeptides in a sensitive hemolytic assay using a highly diluted (4%) solution of human erythrocytes. Peptide acylation increased the hemolytic activity of the lipopeptides. Nevertheless, all the lipopeptides showed either no or low hemolytic activity at their MICs (Table 2).

Oligomeric State and Secondary Structure of the Peptides in Solution Determined by CD Spectroscopy. The effect of the lipophilic acid moiety on the secondary structure and on the oligomeric state of the peptides in PBS was determined by CD spectroscopy at different concentrations (from 10 to 100 μM). A similar spectrum was observed for each peptide independent of the concentration used. Figure 1 presents the CD spectra of the peptides at 100 μM. The data revealed that only [D]-K_5L_7-PA (panel A) and [D]-4-magainin-PA (panel B) adopted well-defined conformations, with major peaks located at wavelengths corresponding to α-helix and β-sheet structures, respectively. [D]-4-magainin-UA also showed a peak at a wavelength corresponding to a β-sheet structure, although significantly lower than that of the palmitoylated analogue. Since monomeric short peptides are not expected to have stable structures in solution, the CD signal indicates the formation of aggregates in aqueous solution, probably via the micellization of the lipophilic acid moiety. Indeed, previous studies showed that the micellar concentration of palmitic acid conjugated to an amino acid is in the micromolar range and should significantly decrease by increasing the peptidic chain (*56*). In contrast, [D]-K_5L_7-UA and its parental peptide showed a typical spectrum of random coils in solution at concentrations up to 100 μM, supporting a nonmicellar organization for these peptides. Lipopeptides that adopted a structure in solution were inactive on most pathogens tested. This indicates that the formation of large aggregates in solution decreases biological activity.

Secondary Structure of the Peptides in Phospholipid Membrane. We used ATR-FTIR to determine the secondary structure of the lipopeptides in phopholipid membranes, described previously in detail (*36*). We examined the IR

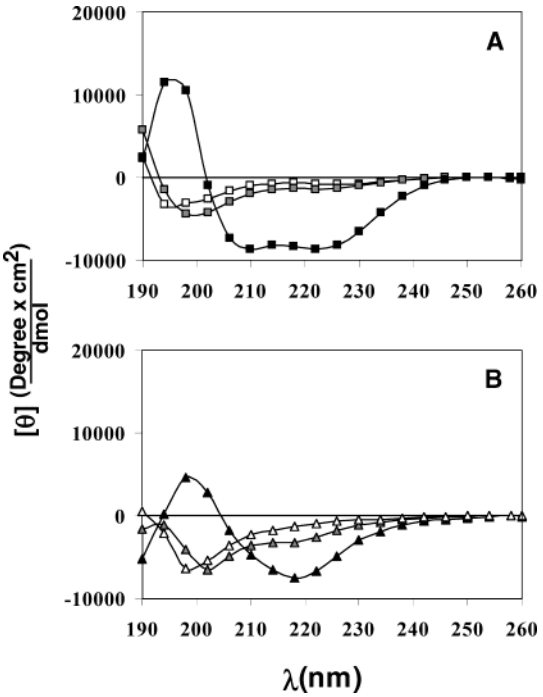

FIGURE 1: CD spectra of the peptides in PBS. Spectra were taken at a peptide concentration of 100 μM. The assay was performed as described in the Materials and Methods section. The designations are as follows: (A) [D]-K_5L_7 (□), [D]-K_5L_7-UA (gray squares), [D]-K_5L_7-PA (■); (B) [D]-4-magainin (△), [D]-4-magainin-UA (gray triangles), [D]-4-magainin-PA (▲).

spectra of the peptides after complete deuteration, which was measured by the complete shift of the amid II band from ~1500 to ~1400 cm^{-1}. PC/PE/PI/ergosterol (5:2.5:2.5:1 w/w/w/w) multibilayers were used at a lipid:peptide molar ratio of 60:1. Figure 2 panels A and C show the amide I region spectra of [D]-K_5L_7 and [D]-4-magainin, together with their UA and PA conjugates, respectively. Second derivatives with Savitsky−Golay smoothing were calculated to identify the positions of the component bands in the spectra and are given in panels B and D of Figure 2. The maxima wavenumbers (υ) taken from the respective second derivatives were used as initial parameters for curve fitting with Gaussian component peaks. The assignments, maxima wavenumbers, and relative areas of the component peaks are summarized in Table 4. Assignment of the different secondary structures to the various amide I regions was calculated according to the values taken from Jackson and Mantsch (*57*). The data reveal that the conjugation of the lipophilic acids to [D]-4-magainin preserved its secondary structure (Figure 2C, Table 4). However, the attachment of the lipophilic acids to [D]-K_5L_7 increased its α-helix/distorted helix fraction, as revealed by a shift of about 7 cm^{-1} from 1666 to 1659 cm^{-1} of the amide I band (Figure 2A, Table 4). Similar wavenumbers were reported for a transmembrane domain of bacteriorhodopsin and other proteins (*53*, *58*). Note that absorption of a normal α-helix in short peptides has also been assigned to higher wavelengths, typically 1660 cm^{-1} for 12 residue peptides (similar to the length of [D]-K_5L_7) (*59*). There is a direct correlation between the increase in the helical content of the lipopeptides and the increase in their biological activity. Thus, the activity of fatty acid-conjugated [D]-K_5L_7 lipopeptides is higher than its parental peptide, whereas the fatty acid-conjugated [D]-4-magainins maintains their parental-like low potency.

Orientation of the Phospholipid Membrane and the Effect of the Peptides on Phospholipid Acyl-Chain Order. Polarized ATR-FTIR spectroscopy was used to determine the orientation of the lipid membrane. The symmetric [$\upsilon_{sym}(CH_2) \approx 2853$ cm^{-1}] and the antisymmetric [$\upsilon_{sym}(CH_2) \approx 2922$ cm^{-1}] vibrations of lipid methylene C−H bonds are perpendicular to the molecular axis of a fully extended hydrocarbon chain. Thus, measurements of the dichroism of infrared light absorbance can reveal the order and orientation of the membrane sample relative to the prism surface. However, since the intensity of the antisymmetric CH_2 vibration was higher than 1, our calculations were based only on *R* values taken from the symmetric vibration. On the basis of the dichroic ratio of lipid stretching, the corresponding order parameter, *f*, was calculated. Antisymmetric (~2922 cm^{-1}) and symmetric peaks (~2853 cm^{-1}) indicate that the membranes are predominantly in a liquid-crystalline phase similar to biological cell membranes (*50*, *60*). The effect of the peptides on the multibilayer acyl-chain orders can be estimated by comparing the CH_2- stretching dichroic ratio of pure phospholipid multibilayers and membrane-bound peptides. The data reveal a significantly more pronounced effect for [D]-K_5L_7 and its aliphatic acid conjugates ($\Delta_{dichroic\ ratio} \approx 0.13$) compared with magainin diastereomer and its analogues ($\Delta_{dichroic\ ratio} \approx 0.21$). In addition, the order parameter, *f*, of each peptide remained the same with or without the conjugation of the lipophilic acids, indicating that lipophilic acid did not change the orientation of the peptides. Overall, there is a good correlation between the biological activity and the effect of the lipopeptides on the lipid order. [D]-K_5L_7-UA and [D]-K_5L_7-PA, which affected the lipid order to the highest extent, were more potent than [D]-4-magainin-UA and [D]-4-magainin-PA.

Peptide-Induced Membrane Destabilization. To determine whether biological activity depends on the ability of the lipopeptides to permeate target membranes, we performed a diffusion potential assay with both living cells and their corresponding model membranes. Both cells and vesicles were preincubated with the fluorescent dye diS-C_3-5. The liposomes were also pretreated with valinomycin in order to create a transmembrane potential.

(*i*) *Membrane Depolarization of Intact Yeast and PC/PE/PI/Ergosterol Vesicles.* Figure 3 shows the dose-dependent dissipation of the transmembrane potential of PC/PE/PI/ergosterol vesicles (panel A) and *C. neoformans* (panel B). The data reveal a similar trend between the ability of the peptides to induce membrane depolarization in intact *C. neoformans* and in its corresponding model membranes. [D]-K_5L_7 derivatives are more active on both systems compared with [D]-4-magainin derivatives. Note that [D]-K_5L_7 -PA is more active on model membranes compared with *C. neoformans*. This might be due to the larger aggregates of [D]-K_5L_7 -PA compared with [D]-K_5L_7 -UA (due to micellization of PA), which should make it more difficult for [D]-K_5L_7 -PA to penetrate through the cell wall of *C. neoformans*.

(*ii*) *Membrane Depolarization of Bacterial Spheroplasts and PE/PG Vesicles.* Figure 4 shows the dose-dependent dissipation of the transmembrane potential of PE/PG vesicles (panel A) and *E. coli* D21 spheroplasts (panel B). A similar

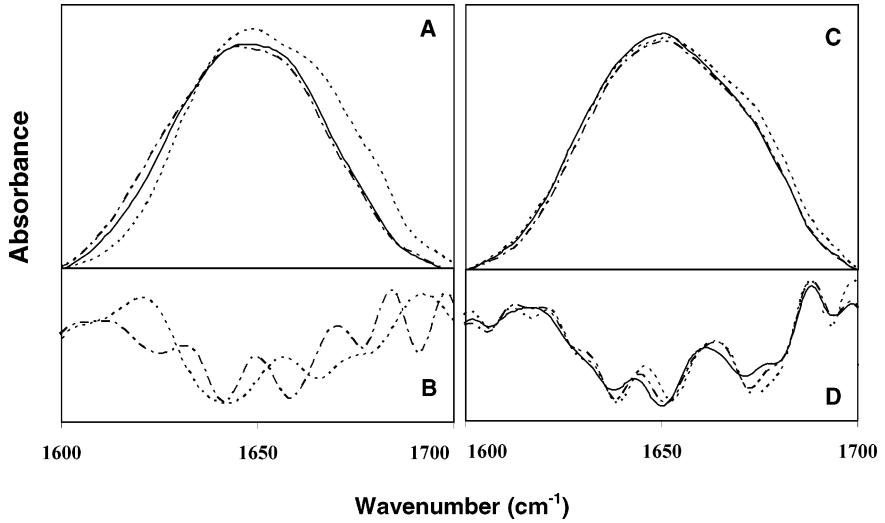

FIGURE 2: FTIR spectra of the fully deuterated amide I band (1600−1700 cm^{-1}) of [D]-K_5L_7 (A) and [D]-4-magainin (C) in PC/PE/PI/ergosterol (5:2.5:2.5:1 w/w/w/w) multibilayers. Second derivatives were calculated to identify the positions of the component bands in the spectra and are presented in panels B and D for K_5L_7 and [D]-4-magainin, respectively. All curves represent the experimental FTIR spectra after Savitzky−Golay smoothing. A 60:1 lipid/diastereomer molar ratio was used. The peptides' designation are parental peptides (---), undecanoyl (− · −), and palmitoyl (—).

Table 4: Assignment and Relative Areas of the Component Peaks as Revealed by ATR-FTIR Spectra[a]

peptide designation	peptide assignment									
	β-sheet 1625−1640 cm^{-1}		random coil 1640−1645 cm^{-1}		α-helix 1650−1654 cm^{-1}		3_{10}-helix 1655−1670 cm^{-1}		β-sheet/turn 1670−1680 cm^{-1}	
	υ (cm^{-1})	area (%)	υ (cm^{-1})	area (%)	υ (cm^{-1})	area (%)	υ (cm^{-1})	area (%)	υ (cm^{-1})	area (%)
[D]-K_5L_7			1640 ± 1	49 ± 2			1666 ± 1	51 ± 1		
[D]-K_5L_7-UA	1625 ± 1	20 ± 2	1642 ± 1	37 ± 2			1659 ± 1	34 ± 4	1676 ± 1	9 ± 1
[D]-K_5L_7-PA	1627 ± 1	23 ± 1	1642 ± 1	31 ± 2			1659 ± 1	39 ± 1	1677 ± 1	7 ± 2
[D]-4-magainin	1636 ± 1	37 ± 1			1654 ± 1	40 ± 2			1674 ± 1	23 ± 1
[D]-4-magainin-UA	1637 ± 1	30 ± 3			1652 ± 1	42 ± 1			1672 ± 1	28 ± 4
[D]-4-magainin-PA	1637 ± 2	31 ± 3			1652 ± 1	41 ± 1			1672 ± 1	28 ± 4

[a] A 1:60 peptide:lipid molar ratio was used. All values are given as mean ± standard deviation. [b] Deconvolution of the amide I bands of the peptides incorporated into PC/PE/PI/ergosterol (5:2.5:2.5 w/w/w) multibilayers. The results are the average of four independent experiments.

inoculum value was used for both the diffusion potential and antimicrobial assays. The data reveal a direct correlation between the ability of all the peptides to dissipate the bacterial transmembrane potential and their ability to increase the permeability of PE/PG vesicles. This suggests that the main target of these peptides is the bacterial plasma membrane. Note, however, that only [D]-K_5L_7 -UA possesses potent activity toward all bacterial stains, which indicates that this peptide is probably the only one that can diffuse through the walls of all bacteria into their cytoplasmic membrane in all strains investigated. Note also that once the cell wall is removed, all the peptides are potent on cytoplasmic membrane.

Electron Microscopy Visualization of Bacterial Lysis. The effect of the lipopeptides on *E. coli* was visualized by using transmission electron microscopy. We used [D]-K_5L_7-UA, which was active on *E. coli*, and [D]-4-magainin-UA, which was not active on this bacterium. At concentrations corresponding to the MIC values, significant differences in the morphology of the treated bacteria were noted (Figure 5). More specifically, [D]-K_5L_7-UA caused damage to the cell wall in the form of blebs (Figure 5B). In contrast, similar morphologies were observed for [D]-4-magainin-UA and for the control sample, which contained only bacteria (Figure 5, panels C and A, respectively).

DISCUSSION

Most cationic antimicrobial peptides have cell-selective activity. Specifically, many of them bind strongly and increase the permeability of negatively charged phospholipid membranes, which are the main components of bacterial plasma membranes (*40*, *61*−*63*). However, their affinity toward zwitterionic membranes, which mimic the membrane of fungi and other eukaryotic cells, is significantly lower. Previous studies have shown that self-association of such peptides confers them with high activity toward zwitterionic membranes and, as a consequence, toward fungi and other eukaryotic cells. In these studies, self-association was induced by amino acid substitutions along the peptide chain (*29*, *31*, *36*) or covalent binding of the monomers (*37*). Such substitutions could change several other properties of these peptides, such as solubility, secondary structure, and mode of action on membranes. In addition, it is difficult to predict the appropriate substitutions for a particular peptide that will trigger its self-association. Recently we have proposed a new approach that allows peptide assembly without altering the peptide backbone sequence. This was done by conjugating lipophilic acids to the N-terminus of the native antibacterial peptide magainin (*38*). Importantly, we found that the peptides' activity and organization depend on the length of the aliphatic chain. Thus, the attachment of undecanoic acid

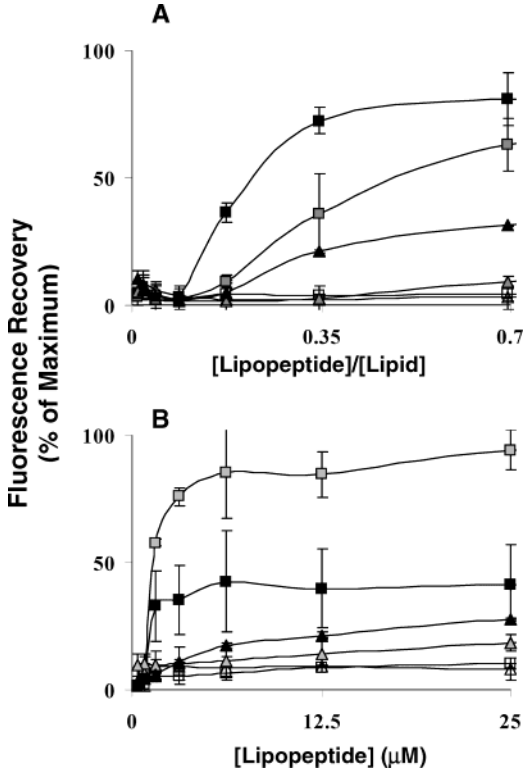

FIGURE 3: Maximal dissipation of the diffusion potential in PC/PE/PI/ergosterol vesicles (A) and intact yeast (B) induced by the lipopeptides. The peptides were added to PC/PE/PI/ergosterol vesicles or *C. neoformans* conidia that were preincubated with the fluorescent dye diS-C_3-5 for 5 min. Membrane depolarization was monitored by an increase in the fluorescence of diS-C_3-5 (excitation wavelength λ_{ex} = 622 nm, emission wavelength λ_{em} = 670 nm) after the addition of peptides at different concentrations. Fluorescence recovery was measured as a function of time at 5−10 min intervals and its maximum was reported. The designations are as follows: [D]-4-magainin-UA (gray triangles), [D]-4-magainin-PA (▲), [D]-K_5L_7 (□), [D]-K_5L_7-UA (gray squares), [D]-K_5L_7-PA (■).

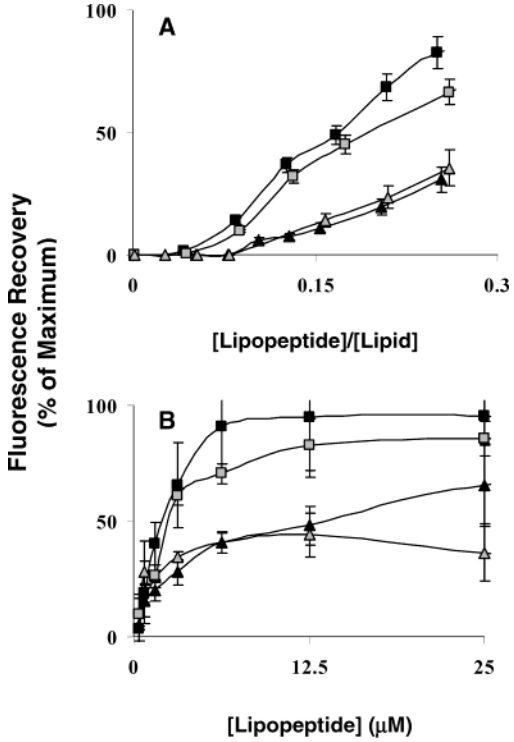

FIGURE 4: Maximal dissipation of the diffusion potential in bacterial PE/PG vesicles (A) and bacteria spheroplasts (B) induced by the peptides. The peptides were added to PE/PG vesicles or *E. coli* spheroplasts that were preincubated with the fluorescent dye diS-C_3-5 for 5 min. Membrane depolarization was monitored by an increase in the fluorescence of diS-C_3-5 (excitation wavelength λ_{ex} = 622 nm, emission wavelength λ_{em} = 670 nm) after the addition of peptides at different concentrations. Fluorescence recovery was measured as a function of time at 5−10 min intervals and its maximum was reported. [D]-4-Magainin was inactive and therefore not shown. The designations are as follows: [D]-4-magainin-UA (gray triangles), [D]-4-magainin-PA (▲), [D]-K_5L_7-UA (gray squares), [D]-K_5L_7-PA (■).

induced oligomerization of magainin, which resulted in increased activity toward fungi and yeast (*38*). In other studies, we have shown that the incorporation of D-amino acids into non-cell-selective lytic peptides preserved the antibacterial activity while decreasing their lytic activity toward eukaryotic cells (*39*, *64*, *65*). This has rendered them with improved properties necessary for therapeutic usage.

In this study, we combined these two approaches and attached undecanoic and palmitic acids to diastereomers of an amphipathic lytic peptide (K_5L_7) and magainin. In contrast to the biologically active all-L-amino acid magainin reported before (*38*), the two diastereomers studied here were practically devoid of antimicrobial activity. One exception was [D]-K_5L_7, which was active toward the highly susceptible pathogens *B. subtilis* and *C. neoformans*. The poor antimicrobial activity is an advantage that allowed us to measure and correlate the effects of lipophilic acid attachment to biological activity, oligomeric state, and interaction with model membranes. Interestingly, we found that all the lipopeptides gained high activity toward *C. neoformans* (Table 2). Furthermore, in contrast to the narrow spectrum of activity of [D]-4-magainin analogues, [D]-K_5L_7 analogues are highly active on a broad spectrum of species (Tables 2 and 3). Most interestingly, [D]-K_5L_7-UA is highly potent toward all microorganisms tested, i.e., bacteria, yeast, and fungi, whereas it has a low hemolytic activity at its MIC (data not shown).

The correlation between the biological function and lipophilic acid attachment will be discussed in the context of two proposed steps involved in the antibacterial and antifungal activity of these lipopeptides: (i) the ability to transverse the cell wall into the cytoplasmic phospholipid membrane and (ii) the ability to interact and increase the permeability of the cytoplasmic membrane.

Different Modes of Lipopeptide Self-Assembly Affect Cell Wall Penetration and Biological Function. CD spectroscopy revealed specifically defined and substantial structures in solution only for the palmitoylated analogues (Figure 1). Since the sequence of the peptide is identical in both the undecanoyl and palmitoyl analogues, the induced structures of the palmitoylated peptides could be either the result of interaction of the peptidic moiety with the lipophilic chain (which is longer and more hydrophobic in the palmitoyl analogue compared with the undecanoyl analogue) or due to the aggregation of the peptidic moieties of several monomers. The FTIR spectroscopy (Figure 2) revealed a marked α-helical structure for both [D]-K_5L_7-PA and [D]-4-magianin-PA in the membranous environment. Therefore, the finding of a β-sheet and not an α-helix for [D]-4-magianin-PA in solution suggests appreciable peptide−peptide interaction in the oligomer in addition to the

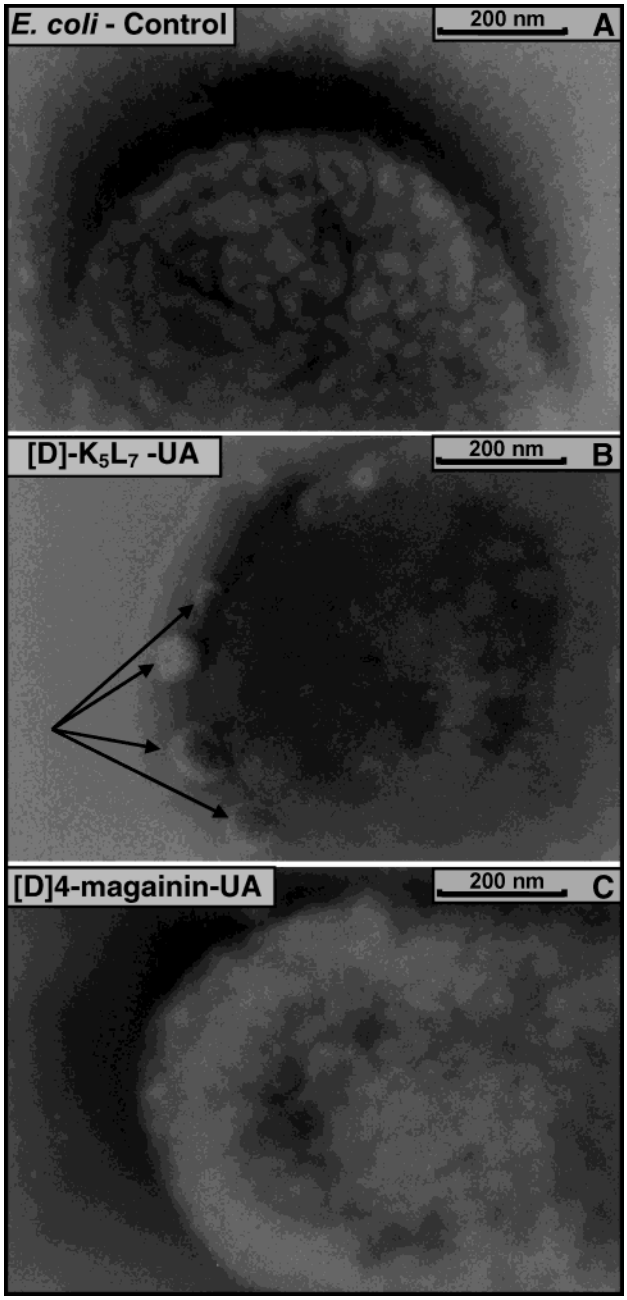

FIGURE 5: Electron micrographs of negatively stained *E. coli* ATCC 25922 untreated and treated with the lipopeptides at their MIC: (A) untreated *E. coli*; (B) *E. coli* treated with [D]-K_5L_7-UA; (C) *E. coli* treated with [D]-4-magainin-UA. Arrows indicate the blebs formed after treatment with [D]-K_5L_7-UA.

micellization of the palmitic moiety. Indeed, [D]-4-magainin-PA was the only peptide that formed β-amyloid fibrils, as seen by transmission electron microscopy (figure not shown). The formation of β-amyloid sheets is a well-known phenomenon in proteins that misfold. In support of this, it has been shown previously that covalently linked pentamers of antimicrobial peptides had a structure of β-sheets, in contrast to the monomers that had a predominantly dynamic helix structure (*37*). Furthermore, whereas no induced structure was observed with [D]-K_5L_7-UA, a partial although small fraction of a β-sheet structure was also observed with [D]-4-magianin-UA (Figure 1). Compared with [D]-4-magianin-PA, [D]-K_5L_7-PA is α-helical in solution. Its induced structure could be the result of both peptide−peptide and peptide−fatty acid interactions. Overall, aggregates of β-sheets are expected to be much larger and therefore more difficult to dissociate compared with α-helical bundles. Therefore, the different mode of oligomerization of the lipophilic peptide analogues of the two diastereomers could explain the differences in their activity. In fact, many pathogens including bacteria, yeast, and fungi are surrounded, in addition to the plasma membrane, by an external barrier, which contains mainly polysaccharide compounds. Therefore, to reach the target phospholipid membranes they need to traverse the microorganism cell wall via a specific uptake pathway. Hancock and co-workers (*66*) termed this process for Gram-negative bacteria a self-promoted uptake. Indeed, there is a direct correlation between the mode of oligomerization and the spectrum of activity, such that the most active one is [D]-K_5L_7-UA, followed by [D]-K_5L_7-PA, [D]-4-magianin-UA, and [D]-4-magianin-PA. It is well-known that echinocandins, which inhibit one of the subunits of 1,3-β-D-glucan synthetase (Fks1p), are not active toward *C. neoformans*, although the synthetase is required for viability (*67*−*69*). Although the mechanism for *C. neoformans* resistance to echinocandins is not yet clear, it may be due to differences in the cell wall structure of this species. In particular, staining with the 1,3-β-D-glucan-specific fluorochrome aniline blue suggests that the 1,3-β-D-glucan component in *Cryptococcus* cell wall is much less prevalent than in *Candida* (*70*). This supports our assumption that the cell wall of *C. neoformans* is more permeable to our lipopeptides, which reach the plasma membrane and disrupt it. Although the echinocandins, especially caspofungin, were approved by the FDA for therapeutic usage (*22*, *23*), they are limited mostly to *Candida* and *Aspergillus* species, while the cryptococcal disease remains uncovered by these drugs. Thus, further study on our lipopeptides, which are highly active toward *C. neoformans*, should assist in the development of broad-spectrum antifungal agents.

Major Target of the Lipopeptides Is the Cytoplasmic Phospholipid Membrane. As soon as the peptides cross the cell wall of the pathogen, the major barrier left is the plasma membrane. The data suggest that the major target of the lipopeptides is the microorganism membrane. This assumption is supported by the direct correlation between the potency of the lipopeptides to increase the permeability of bacteria spheroplasts (lacking the outer wall) and the permeable *C. neoformans* and their corresponding model membranes (Figures 3 and 4). A good correlation was also found between transmembrane potential depolarization (Figures 3 and 4) and the ability of the peptides to alter the membrane order (ATR-FTIR data, Results section). Fatty acid-conjugated [D]-K_5L_7 peptides disturb the acyl chain order to a greater extent than fatty acid-conjugated [D]-4-magianin, in agreement with their higher activity in the dissipation of diffusion potential experiments. Previous studies with all-L-amino acid magainin and its three lipophilic acid conjugates revealed that the ability of the lipopeptides to destabilize PC/PE/PI/ergosterol vesicles correlated with the length of the attached lipophilic acid (*38*). This could be explained by increased affinity of the lipopeptides to vesicles as a result of hydrophobic interactions, which was supported by earlier studies of Peitzsch and McLaughlin (*71*) by using anionic forms of fatty acids and the corresponding acylated glycines or tripeptides. It was also shown that, once bound,

all three lipomagainins were oriented parallel to the membrane surface and altered the membrane order, similarly to the parental peptide magainin (*38*). Here we obtained similar results with [D]-4-magianin analogues. The [D]-K_5L_7 analogues induced a more pronounced effect on the acyl chain order, the reason for which is not yet clear but might be due to the different hydrophobicities of the peptides and their structures in the membrane (Table 4, Figure 2). The EM studies also confirm that physical damage to the bacteria took place after the application of active [D]-K_5L_7-UA and not the inactive [D]-4-magianin-UA (Figure 5B and C).

Most natural antifungal lipopeptides are unusually short (6−7 amino acids), cyclic (*18*), negatively charged, and mainly hydrophobic and are composed of acidic L- and D-amino acid compositions. They have been shown to act via two major different mechanisms (*72*): (i) by inhibiting the synthesis of cell wall components such as (1,3)-β-D-glucan or chitin (*73*, *74*) and (ii) by membrane lysis, although the details are unknown (e.g., iturins, bacillomycin, and surfactin) (*19*, *75*, *76*). The biophysical studies presented here, together with the findings of a direct correlation between the MIC and the in vitro and in vivo transmembrane potential depolarization assays with the permeable *C. neoformans*, along with the EM studies suggest that the lipopeptides act directly on the cell plasma membrane. However, they must cross the cell wall prior to reaching the inner membrane, which is more difficult for peptides that form high-order oligomers, which are not readily dissociable.

Besides shedding light on the parameters that affect the activity of the present lipopeptides, this study paves the way to develop a new promising group of lipopeptide candidates for therapeutic use against a broad spectrum of microorganisms including fungi, yeast, and bacteria. The incorporation of D-amino acids should give these peptides several advantages over their all-L-amino acid counterparts, such as controlled enzymatic degradation, as has been shown recently for diastereomeric antibacterial peptides (*39*).

REFERENCES

1. Denning, D. W. (1991) *J. Antimicrob. Chemother. 28*, 1−16.
2. Ellis, M., Richardson, M., and de Pauw, B. (2000) *Hosp. Med. 61*, 605−609.
3. Odds, F. C., Brown, A. J., and Gow, N. A. (2003) *Trends Microbiol. 11*, 272−279.
4. Sheehan, D. J., Hitchcock, C. A., and Sibley, C. M. (1999) *Clin. Microbiol. Rev. 12*, 40−79.
5. Kullberg, B. J., and de Pauw, B. E. (1999) *Neth. J. Med. 55*, 118−127.
6. Alexander, B. D., and Perfect, J. R. (1997) *Drugs 54*, 657−678.
7. Mukherjee, P. K., Chandra, J., Kuhn, D. M., and Ghannoum, M. A. (2003) *Infect. Immun. 71*, 4333−4340.
8. Kontoyiannis, D. P., Mantadakis, E., and Samonis, G. (2003) *J. Hosp. Infect. 53*, 243−258.
9. Arima, K., Kakinuma, A., and Tamura, G. (1968) *Biochem. Biophys. Res. Commun. 31*, 488−494.
10. Bernheimer, A. W., and Avigad, L. S. (1970) *J. Gen. Microbiol. 61*, 361−369.
11. Vollenbroich, D., Ozel, M., Vater, J., Kamp, R. M., and Pauli, G. (1997) *Biologicals 25*, 289−297.
12. Pankuch, G. A., Jacobs, M. R., and Appelbaum, P. C. (2003) *J. Antimicrob. Chemother. 51*, 443−446.
13. Goldstein, E. J., Citron, D. M., Merriam, C. V., Warren, Y. A., Tyrrell, K. L., and Fernandez, H. T. (2003) *Antimicrob. Agents. Chemother. 47*, 337−341.
14. BenMohamed, L., Wechsler, S. L., and Nesburn, A. B. (2002) *Lancet Infect. Dis. 2*, 425−431.
15. Fiechter, A. (1992) *Trends Biotechnol. 10*, 208−217.
16. Kim, S. H., Lim, E. J., Lee, S. O., Lee, J. D., and Lee, T. H. (2000) *Biotechnol. Appl. Biochem. 31*, 249−253.
17. Ron, E. Z., and Rosenberg, E. (2001) *Environ. Microbiol. 3*, 229−236.
18. De Lucca, A. J., and Walsh, T. J. (1999) *Antimicrob. Agents Chemother. 43*, 1−11.
19. Maget-Dana, R., and Peypoux, F. (1994) *Toxicology 87*, 151−174.
20. Heerklotz, H., and Seelig, J. (2001) *Biophys. J. 81*, 1547−1554.
21. Wiederhold, N. P., and Lewis, R. E. (2003) *Expert Opin. Invest. Drugs 12*, 1313−1333.
22. Johnson, M. D., and Perfect, J. R. (2003) *Expert Opin. Pharmacother. 4*, 807−823.
23. Kartsonis, N. A., Nielsen, J., and Douglas, C. M. (2003) *Drug Resist. Update 6*, 197−218.
24. Boman, H. G. (1991) *Cell 65*, 205−207.
25. Nicolas, P., and Mor, A. (1995) *Annu. Rev. Microbiol. 49*, 277−304.
26. Lehrer, R. I., and Ganz, T. (1999) *Curr. Opin. Immunol. 11*, 23−27.
27. Hancock, R. E., and Diamond, G. (2000) *Trends Microbiol. 8*, 402−410.
28. Zasloff, M. (1987) *Proc. Natl. Acad. Sci. U.S.A. 84*, 5449−5453.
29. Ghosh, J. K., Shaool, D., Guillaud, P., Ciceron, L., Mazier, D., Kustanovich, I., Shai, Y., and Mor, A. (1997) *J. Biol. Chem. 272*, 31609−31616.
30. Bulet, P., Hetru, C., Dimarcq, J. L., and Hoffmann, D. (1999) *Dev. Comput. Immunol. 23*, 329−344.
31. Kustanovich, I., Shalev, D. E., Mikhlin, M., Gaidukov, L., and Mor, A. (2002) *J. Biol. Chem. 277*, 16941−16951.
32. Lupetti, A., Danesi, R., van't Wout, J. W., van Dissel, J. T., Senesi, S., and Nibbering, P. H. (2002) *Expert Opin. Invest. Drugs 11*, 309−3018.
33. Romestand, B., Molina, F., Richard, V., Roch, P., and Granier, C. (2003) *Eur. J. Biochem. 270*, 2805−2813.
34. Shai, Y. (2002) *Biopolymers 66*, 236−248.
35. Strahilevitz, J., Mor, A., Nicolas, P., and Shai, Y. (1994) *Biochemistry 33*, 10951−10960.
36. Oren, Z., Lerman, J. C., Gudmundsson, G. H., Agerberth, B., and Shai, Y. (1999) *Biochem. J. 341*, 501−513.
37. Sal-Man, N., Oren, Z., and Shai, Y. (2002) *Biochemistry 41*, 11921−11930.
38. Avrahami, D., and Shai, Y. (2002) *Biochemistry 41*, 2254−2263.
39. Papo, N., Oren, Z., Pag, U., Sahl, H. G., and Shai, Y. (2002) *J. Biol. Chem. 277*, 33913−33921.
40. Shai, Y. (2002) *Curr. Pharm. Des. 8*, 715−725.
41. Shai, Y., Bach, D., and Yanovsky, A. (1990) *J. Biol. Chem. 265*, 20202−20209.
42. Schneiter, R., Brugger, B., Sandhoff, R., Zellnig, G., Leber, A., Lampl, M., Athenstaedt, K., Hrastnik, C., Eder, S., Daum, G., Paltauf, F., Wieland, F. T., and Kohlwein, S. D. (1999) *J. Cell. Biol. 146*, 741−754.
43. Wu, C. S., Ikeda, K., and Yang, J. T. (1981) *Biochemistry 20*, 566−570.
44. Greenfield, N., and Fasman, G. D. (1969) *Biochemistry 8*, 4108−4116.
45. Sims, P. J., Waggoner, A. S., Wang, C. H., and Hoffmann, J. R. (1974) *Biochemistry 13*, 3315−3330.
46. Loew, L. M., Rosenberg, I., Bridge, M., and Gitler, C. (1983) *Biochemistry 22*, 837−844.
47. Frate, M. C., Lietz, E. J., Santos, J., Rossi, J. P., Fink, A. L., and Ermacora, M. R. (2000) *Eur. J. Biochem. 267*, 3836−3847.
48. Gazit, E., Miller, I. R., Biggin, P. C., Sansom, M. S. P., and Shai, Y. (1996) *J. Mol. Biol. 258*, 860−870.
49. Surewicz, W. K., Mantsch, H. H., and Chapman, D. (1993) *Biochemistry 32*, 389−394.
50. Ishiguro, R., Kimura, N., and Takahashi, S. (1993) *Biochemistry 32*, 9792−9797.
51. Harrick, N. J. (1967) *Internal Reflection Spectroscopy*, New York ed., Interscience, New York.
52. Tamm, L. K., and Tatulian, S. A. (1997) *Q. Rev. Biophys. 30*, 365−429.
53. Rothschild, K. J., and Clark, N. A. (1979) *Science 204*, 311−312.
54. Bradbury, E. M., Brown, L., Downie, A. R., Elliott, A., Fraser, R. D. B., and Hanby, W. E. (1962) *J. Mol. Biol 5*, 230−147.
55. Schiffer, M., and Edmundson, A. B. (1967) *Biophys. J. 7*, 121−135.

56. Shinitzky, M., and Haimovitz, R. (1993) *J. Am. Chem. Soc. 115*, 12545−12549.
57. Jackson, M., and Mantsch, H. H. (1995) *Crit. Rev. Biochem. Mol. Biol. 30*, 95−120.
58. Dwivedi, A. M., and Krimm, S. (1984) *Biopolymers 23*, 923−943.
59. Goormaghtigh, E., Vigneron, L., Scarborough, G. A., and Ruysschaert, J. M. (1994) *J. Biol. Chem. 269*, 27409−27413.
60. Cameron, D. G., Casal, H. L., Gudgin, E. F., and Mantsch, H. H. (1980) *Biochim. Biophys. Acta 596*, 463−467.
61. Matsuzaki, K. (1999) *Biochim. Biophys. Acta 1462*, 1−10.
62. Zasloff, M. (2002) *Nature 415*, 389−395.
63. Hancock, R. E., and Rozek, A. (2002) *FEMS Microbiol. Lett. 206*, 143−149.
64. Shai, Y., and Oren, Z. (1996) *J. Biol. Chem. 271*, 7305−8.
65. Oren, Z., and Shai, Y. (1997) *Biochemistry 36*, 1826−3518.
66. Sawyer, J. G., Martin, N. L., and Hancock, R. E. (1988) *Infect. Immun. 56*, 693−698.
67. Bartizal, K., Abruzzo, G., Trainor, C., Krupa, D., Nollstadt, K., Schmatz, D., Schwartz, R., Hammond, M., Balkovec, J., and Vanmiddlesworth, F. (1992) *Antimicrob. Agents Chemother. 36*, 1648−1657.
68. Krishnarao, T. V., and Galgiani, J. N. (1997) *Antimicrob. Agents. Chemother. 41*, 1957−1960.
69. Thompson, J. R., Douglas, C. M., Li, W., Jue, C. K., Pramanik, B., Yuan, X., Rude, T. H., Toffaletti, D. L., Perfect, J. R., and Kurtz, M. (1999) *J. Bacteriol. 181*, 444−453.
70. Nicholas, R., Williams, D., and Hunter, P. (1994) *Mycol. Res. 98*, 694−698.
71. Peitzsch, R. M., and McLaughlin, S. (1993) *Biochemistry 32*, 10436−10443.
72. Loeffler, J., and Stevens, D. A. (2003) *Clin. Infect. Dis. 36*, S31−41.
73. Debono, M., and Gordee, R. S. (1994) *Annu. Rev. Microbiol. 48*, 471−497.
74. Kurtz, M. B., Douglas, C., Marrinan, J., Nollstadt, K., Onishi, J., Dreikorn, S., Milligan, J., Mandala, S., Thompson, J., Balkovec, J. M., and et al. (1994) *Antimicrob. Agents. Chemother. 38*, 2750−2757.
75. Maget-Dana, R., and Ptak, M. (1995) *Biophys. J. 68*, 1937−1943.
76. Peypoux, F., Bonmatin, J. M., and Wallach, J. (1999) *Appl. Microbiol. Biotechnol. 51*, 553−563.

BI035142V